



# Effect of laser repetition rate on the growth of $\text{Sc}_2\text{O}_3$ via pulsed laser deposition

Goby A. Govindassamy<sup>1</sup> · Jake J. Prentice<sup>1</sup> · James. G. Lunney<sup>2</sup> · Robert W. Eason<sup>1</sup> · Jacob I. Mackenzie<sup>1</sup>

Received: 24 November 2021 / Accepted: 16 May 2022 / Published online: 15 June 2022  
© The Author(s) 2022

## Abstract

This paper reports a study of the effect of laser pulse repetition rate and substrate temperature on the properties of crystalline  $\text{Sc}_2\text{O}_3$  films grown on  $\langle 0001 \rangle$ -oriented sapphire via pulsed laser deposition (PLD). For the range of substrate laser-heating powers investigated, optimum  $\langle 111 \rangle$ -film growth was obtained at the highest available repetition rate of 100 Hz. Scanning electron microscopy and X-ray diffraction measurements revealed that a decrease in the repetition rate favours highly textured/island growth. The repetition rate was also proven to affect the lattice constant of the films, with a difference up to 0.3% between the films grown at high and low repetition rates. The general trend indicates that the out-of-plane lattice constant of the film shifts closer to the bulk value when the pulse repetition rate is increased. However, the lattice constant could also be reduced through in-situ post-growth annealing, which had the additional benefit of reducing the width of the (222) rocking curve peak. This work provides further evidence that energetic-PLD dynamics leads to higher quality PLD-grown crystalline films and for this material undermines the old adage that lower pulse repetition rates lead to higher quality thin-film crystalline growth.

**Keywords** Pulsed laser deposition · Thin film · Crystal growth · Sesquioxide · Repetition rate ·  $\text{Sc}_2\text{O}_3$

## 1 Introduction

Scandium oxide ( $\text{Sc}_2\text{O}_3$ ) films have been used in a wide range of optical and electronics applications. Exploiting its wide optical transmission bandwidth (0.21–8  $\mu\text{m}$ ), high thermal conductivity (18  $\text{Wm}^{-1}\text{K}^{-1}$ ), and ability to host rare-earth ions, crystalline  $\text{Sc}_2\text{O}_3$  has been investigated in various waveguide and thin-disk laser formats [1–5]. Moreover, amorphous  $\text{Sc}_2\text{O}_3$  films have been incorporated into both anti- and high-reflection optical coatings [6–8], including those catering for the UV-wavelength regime. The material's high-energy band gap (5.8 eV), and resilience to higher power operating regimes than conventional dielectric materials, was demonstrated for coatings based on pairs of  $\text{Sc}_2\text{O}_3$ /

$\text{SiO}_2$  layers having a 30% higher laser-damage threshold than comparable  $\text{HfO}_2/\text{SiO}_2$  coatings [8]. In electronics,  $\text{Sc}_2\text{O}_3$  and  $\text{Gd}_2\text{O}_3$  were investigated as potential gate dielectrics in metal-oxide semiconductors for GaN devices [9–12]. Their high dielectric constant and good thermal stability led to a lower gate leakage current, and hence a higher voltage breakdown. Moreover,  $\text{Sc}_2\text{O}_3$  has the advantage of having a better lattice match with GaN compared to  $\text{Gd}_2\text{O}_3$  (9.2 and 20% mismatch, respectively), which minimises the number of defects at the interface [9]. The properties of  $\text{Sc}_2\text{O}_3$  make it particularly interesting for our intended application, namely the fabrication of crystalline dielectric mirrors with potentially excellent laser-damage resistance that will enable their operation with high average- and peak-power lasers [13].

Pulsed laser deposition (PLD) is a method of choice for the rapid synthesis of sesquioxide films, as it enables the fabrication of crystalline layers at a temperature around half of the melting point of their bulk-material counterparts [4]. In particular,  $\text{Sc}_2\text{O}_3$  films have been grown via PLD for various photonic, electronic, and quantum technology applications [2, 4, 14, 15]. To date, parametric optimisation has shed light on the influence of the

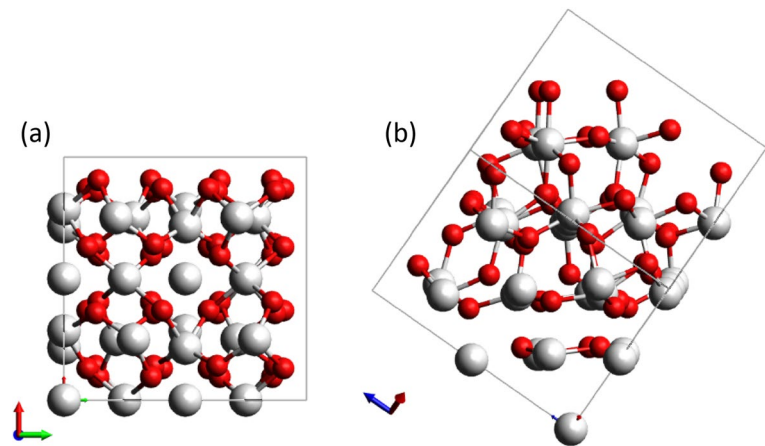
✉ Goby A. Govindassamy  
G.A.Govindassamy@soton.ac.uk

Jacob I. Mackenzie  
jim@soton.ac.uk

<sup>1</sup> Optoelectronics Research Centre, University of Southampton, Southampton SO17 1BJ, UK

<sup>2</sup> School of Physics, Trinity College Dublin, College Green, Dublin 2, Ireland

**Fig. 1** Schematic of the  $\text{Sc}_2\text{O}_3$  unit cell [25], viewed **a** along the  $\langle 001 \rangle$  axis and **b** perpendicular to the vertical  $\langle 111 \rangle$  axis. Frame indicates the unit cell, containing 32 scandium atoms (grey) and 48 oxygen atoms (red)



substrate temperature and background gas pressure [16], target ablation fluence [4], and other key parameters on the growth of sesquioxides. One important parameter in PLD, which has received far less attention so far, is the role and effect of the repetition rate of the laser used to ablate the target.

Several studies indicate the existence of two distinct energetic processes in PLD that determine the mobility of the adatoms on the sample's surface and mechanisms for the resultant 2D or 3D growth [17–19]. Although these reports are for the perovskite family of oxides, of which  $\text{SrTiO}_3$  (STO) is commonly used as an exemplar system, they show that 2D or “layer-by-layer” growth is achievable by favouring conditions that frustrate Ostwald island ripening. Blank et al. [20] demonstrated that delivering sufficient material to the sample's surface to complete a unit cell in a short time interval, i.e., on order of a “characteristic relaxation time”, can mitigate multi-level 2D (3D) growth. A reduction of this characteristic relaxation time is observed with increasing surface temperature, which in turns lowers the probability of interlayer transport, favouring 3D-island growth. In that work, improved layer-by-layer STO-growth was achieved whilst monitoring, via in-situ reflection high-energy electron diffraction (RHEED), island ripening during the intervals between ‘bursts’ of pulses (at 10 Hz). Additionally, Eres et al. [21] quantified the respective time constants for initial crystallisation of the arriving plume species and subsequent redistribution between respective layers, with the help of time-resolved surface X-ray diffraction (SXRD) measurements. When the diffusion time of the adatoms was limited by reducing the intervals between plasma plumes (down to 200 ms), the authors observed that the relative contribution of the slower interlayer transport decreased, and layer-by-layer growth was favoured. Furthermore, the authors stated that the resultant surface morphology is defined by the non-equilibrium transients, which if optimised can prevent the undesirable thermally driven processes that encourage island ripening, and therefore, consequent 3D growth.

This paper focuses on the deposition of  $\text{Sc}_2\text{O}_3$  films on  $\langle 0001 \rangle$ -orientated sapphire substrates, with emphasis on the effects of laser repetition rate, hence the inter-pulse time, and substrate temperature. The impact of these parameters on the crystallinity of the resulting films was analysed to determine an optimal approach for improving the optical quality of the deposited layer. A deeper understanding of the mechanisms involved in the deposition of  $\text{Sc}_2\text{O}_3$  will pave the way for the fabrication of hard-crystal multilayers, and specifically high-quality crystalline Bragg mirrors.

## 2 Methodology

### 2.1 Crystallographic considerations

Despite their very different crystal structure, the cubic phase of  $\text{Sc}_2\text{O}_3$  can grow epitaxially on the trigonal lattice of  $\alpha\text{-Al}_2\text{O}_3$  [2]. More precisely, the  $\langle 111 \rangle$ -orientation of  $\text{Sc}_2\text{O}_3$  presents a threefold rotational symmetry similar to  $\langle 0001 \rangle$  ( $\alpha\text{-Al}_2\text{O}_3$ ). This orientation has a quasi-lattice match with the substrate following the rule of  $3 \times a_{\alpha\text{-Al}_2\text{O}_3} \approx \sqrt{2} \times a_{\text{Sc}_2\text{O}_3}$ , with  $a_{\alpha\text{-Al}_2\text{O}_3} = 0.4758\text{nm}$  the lattice parameter in the (0001)-plane of  $\alpha\text{-Al}_2\text{O}_3$  and  $a_{\text{Sc}_2\text{O}_3} = 0.9846\text{nm}$  the lattice parameter for the cubic  $\text{Sc}_2\text{O}_3$  crystal. Correspondingly, there is only a mismatch of 2.5% [2, 24], which is the smallest among all the orientations of  $\text{Sc}_2\text{O}_3$ . It is thus expected to be the preferred orientation for the resultant epitaxial growth if presented with an ideal (0001)-plane  $\alpha\text{-Al}_2\text{O}_3$  surface.

A key difference for our work presented here, with respect to  $\text{SrTiO}_3$  growth [17, 18], is that  $\text{Sc}_2\text{O}_3$  has a ~3-times larger crystal structure [25]. The unit cell comprising bilayers of scandium and oxygen atoms is shown in Fig. 1a looking along the [001]-axis. Figure 1b illustrates the crystal planes corresponding to  $\langle 111 \rangle$ -growth, as obtained under optimal deposition conditions discussed in the next sections, showing a periodic layering of the scandium atoms.

On average these Sc-atom layers are spaced by 0.284 nm, whilst the oxygen atoms are not as strongly confined to a 'layer' between them.

## 2.2 Experimental setup

All depositions detailed in this study were performed using the PLD setup detailed in [22]. However, as a brief summary, for target ablation, we use a KrF excimer laser (Coherent COMPexPro 110) operating at 248 nm, with a pulse duration of ~20 ns and repetition rate that is variable from 1 to 100 Hz. The pulsed UV laser beam subtends an angle of incidence of 45° to the target and was focussed to a rectangular spot with an area of (7.5 ± 0.2) mm<sup>2</sup> at the target surface. The Sc<sub>2</sub>O<sub>3</sub> ceramic target was sourced from the manufacturer Testbourne Ltd, fabricated by hot pressing 99.99%-purity powder to a density of ~85% of the native oxide. The same target was used for all depositions to avoid any differences between targets. Deposition was made onto double-side epitaxy-ready polished c-cut sapphire substrates (10 × 10 × 1 mm) that were positioned in front of the target at a distance of (55 ± 1) mm. A CO<sub>2</sub> laser, operating at a wavelength of 10.6 μm, heats the substrate from the rear side. A ZnSe tetraprism is used to transform the Gaussian intensity distribution of the CO<sub>2</sub> laser beam into a quasi-top-hat square profile of full width equal to the substrate width [23], which ensured minimal temperature gradients are present across the surface of the substrate facing the target.

A systematic procedure was followed for all the growths, starting with evacuation of the chamber to a pressure of 10<sup>-3</sup> mbar, before introducing oxygen to reach a pressure of 2 × 10<sup>-2</sup> mbar. The temperature of the substrate was then progressively increased to the required value by ramping up the incident CO<sub>2</sub> laser power at a rate of 2 W/min. Pre-ablation of the Sc<sub>2</sub>O<sub>3</sub> target was performed to remove any undesirable surface contamination before each deposition. This involved an 18,000-pulse run, at equivalent parameters used for the actual deposition, whilst shielding the substrate. After each growth run, the CO<sub>2</sub> laser power was gradually ramped down at a rate of 0.5 W/min, minimising the risk of the sample cracking due to thermal stress.

A preliminary optimisation of the deposition parameters was performed at a laser repetition rate of 100 Hz. The crystallinity of the as-grown films was characterised by X-ray diffraction (XRD). Spectra were measured with a Rigaku SmartLab diffractometer equipped with an in-plane arm, a 9 kW (45 kV, 200 mA) Cu target rotating anode generator, and a HyPix 3000 semiconductor detector set to 1D mode. The Cross-Beam-Optics were in the parallel-beam configuration, with 5.0° primary and secondary axial Soller slits, whilst the source was equipped with a Ge(220) 2-bounce monochromator. Optimisation of the growth conditions was based on maximising the height of the Sc<sub>2</sub>O<sub>3</sub> (222)-peak,

which is our orientation of interest, whilst minimising the presence of other crystal orientations. At 100 Hz, an excimer laser fluence of 1.1 J/cm<sup>2</sup> and a CO<sub>2</sub>-laser power of 23–24 W were determined to be the best parameters for the growth of Sc<sub>2</sub>O<sub>3</sub> in our setup. Multiple samples were grown with the optimal excimer laser fluence, at a variety of pulse repetition rates ranging from 1 to 100 Hz. To account for the decrease in the plasma-heating contribution at the lower repetition rates, three sets of samples were grown with three different incident powers for the CO<sub>2</sub> heating laser: 23 ± 0.5 W, 27 ± 0.5 W and 29.5 ± 0.6 W (the quoted error corresponds to the RMS fluctuations of the laser power). The PLD chamber used is devoid of internal diagnostics; however, through prior studies [26] and simulation, the estimated temperature of the substrates for the respective heating powers were (1100 ± 25) °C, (1150 ± 25) °C, and (1200 ± 25) °C. Note that an additional level of uncertainty is added due to the difficulty is assessing the heat-sinking effect of the mount for individual samples. Each deposition was run with 18,000 laser pulses, leading to films ~1-μm thick. To avoid any systematic error related to the degradation of the target, the order of the growths (in terms of selected repetition rate) was randomised.

## 3 Results and discussion

Three key observations will be presented in this section. First, the repetition rate was observed to define whether the film would grow with a smooth or textured surface morphology, evidenced by scanning electron microscopy (SEM) and XRD characterisation. Second, the pulse repetition rate was found to have a strong impact on the predominance of the <111>-orientation of the film. Finally, the XRD-2θ (222)-peak position increased with decreasing ablation frequency, regardless of the other deposition parameters.

### 3.1 Surface morphology

To investigate the morphology of the grown films, SEM images of the growth surface for key samples have been recorded with backscattered electron detection (Zeiss microscope, model EVO50XVP equipped with a CZ BSD detector). Figure 2a–c represents films grown with 23 W of CO<sub>2</sub> laser power incident on the substrate, and Fig. 2d–f corresponds to films deposited on a substrate heated with 29.5 W. For both heating power levels, the density and size of defects in the grown film increased as the deposition frequency decreased, progressing from left to right in Fig. 2. Importantly, the film deposited at 100 Hz with a CO<sub>2</sub> laser power of 23 W is the only one that presents a uniform and compact surface (Fig. 2a).



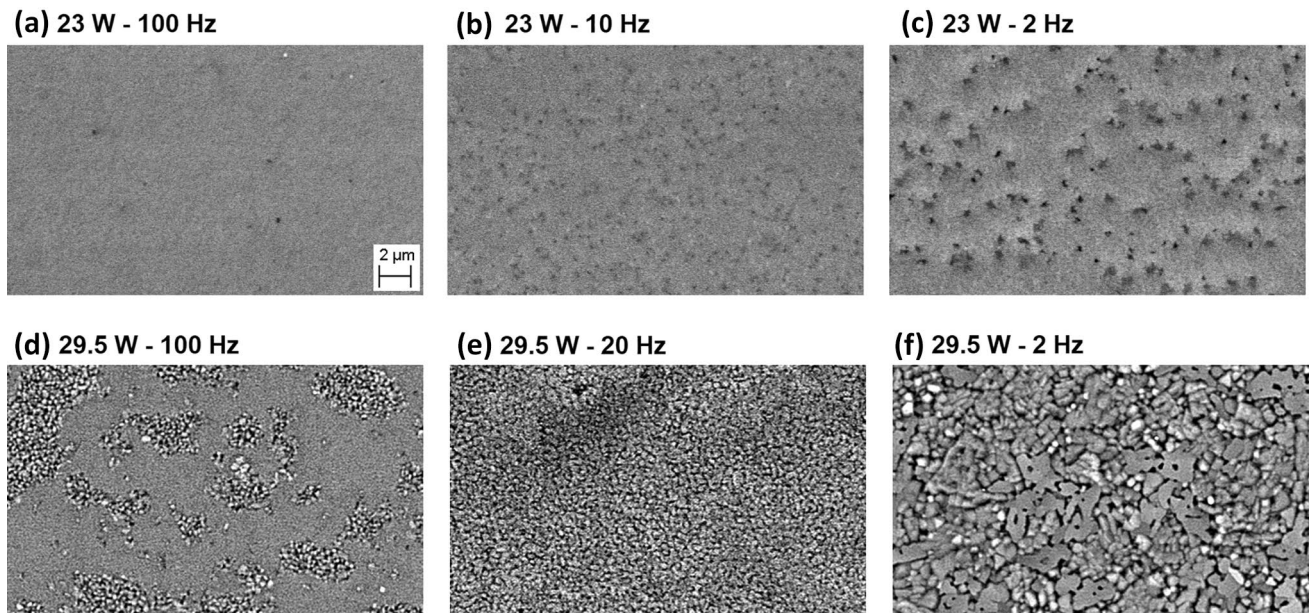


**Fig. 2** SEM images of  $\text{Sc}_2\text{O}_3$  films deposited with the substrate heated by an incident  $\text{CO}_2$  laser power ablation-pulse repetition rate of **a** 23 W–100 Hz, **b** 23 W–10 Hz, **c** 23 W–2 Hz, **d** 29.5 W–100 Hz,

**e** 29.5 W–20 Hz, and **f** 29.5 W–2 Hz. All the images were captured with the same magnification of 5000 $\times$  and the scale bar in **a** is the same for all

From the images in Fig. 2, it is evident that decreasing the repetition rate (left to right in the rows) leads to larger domains (islands) in addition to an increasing number, and size, of ‘voids’ at the surface. Domains are, by definition, regions of independent and uncorrelated growth habit. The discontinuity of the crystal at the interface between domains allows small variations of lattice constant between them. Furthermore, highly textured growth becomes dominant for increasing heating (top to bottom in the columns of Fig. 2), which corroborates the proposition that both surface temperature and plume dynamics are responsible for the final topology of the film.

Blank et al. [20] conducted their study of  $\text{SrTiO}_3$  with a burst-pulse repetition rate of 10 Hz and a typical deposition temperature around 800 °C, measuring a relaxation time on the order of a few-hundred ms, which decreased with increasing surface temperature. Their objective was to use a sufficiently fast growth rate to complete a monolayer within the relaxation time, which would limit the average size of the 2D islands in that layer. This would in turn mitigate 3D-island growth owing to the smaller diffusion distance required for interlayer transport. A number of 27 pulses were required to complete a unit-cell layer with their deposition conditions, corresponding to a growth rate of 0.014 nm/pulse or 2.7 s per unit-cell layer, which was enough to frustrate 3D growth despite still being longer than the measured characteristic relaxation time. In our case, for an incident substrate heating power of 23 W (which we estimate heats it to  $\sim 1100$  °C) and a chamber pressure of  $2 \times 10^{-2}$  mbar, the

crystal growth rate was 0.056 nm/pulse. As such, five pulses (i.e., 50 ms for 100 Hz deposition) were required to provide enough atoms to complete a Sc-O ‘layer’ and 30 pulses for a complete unit-cell layer. For a ‘monolayer’ deposition referring to each of these Sc-O layers, the diffusion time between pulses is an order of magnitude shorter than those exploited for  $\text{SrTiO}_3$  growth. Assuming a similar behaviour in the case of  $\text{Sc}_2\text{O}_3$ , a decrease in ablation-pulse period (increase in deposition frequency) may restrict the Ostwald ripening of 3D islands favouring layer-by-layer growth. This is in good agreement with our observations in Fig. 2 where it is evident that the use of a high ablation-pulse period (low repetition rate) enabled 3D growth, whilst continuous operation with the optimal parameters at 100 Hz deposition leads to smoother films just as illustrated by Pulsed Laser Interval Deposition [20]. Furthermore, the enhancement of 3D growth for higher substrate temperatures supports the idea of a decreasing relaxation time with increasing temperature thus a shortening of time available to complete a monolayer, which was observed with  $\text{SrTiO}_3$  by Blank et al.

Recently, Ulbrandt et al. [18] confirmed that the impingement of energetic plasma, with kinetic energy on the order of  $\sim 100$  eV, is responsible for the breakup of coalescing islands into smaller ones, providing a greater density of edges for nucleation sites. They showed that the nucleation length scale,  $l$ , is significantly smaller for energetic PLD with respect to the equivalent conditions with a thermalised plume, the latter achieved by introducing 300 mTorr of helium into the PLD chamber. In that case, the kinetic

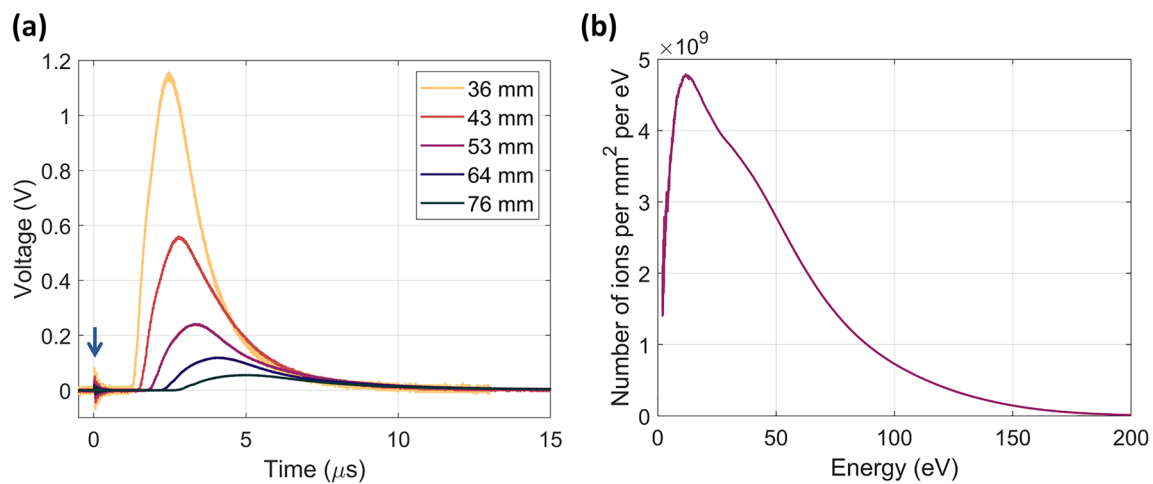


**Fig. 3** **a** Ion probe signals collected for different target-probe distances. The pre-pulses, highlighted by the blue arrow, indicate the arrival of the UV pulses in the chamber and were used as a reference for time zero. **b** Energy distribution of the ions for a target-probe distance of 53 mm.

energy of the incident plasma was on the order of 0.1 eV. The authors demonstrated that energetic PLD suppressed coarsening of the surface and that a reducing dwell time between pulses enhanced this characteristic.

To verify the kinetic energy of the impinging plasma in our experiment, the velocity of the plume front was measured with a planar Langmuir probe, in the form of a  $2 \times 3$  mm copper plate, placed at different distances from the target. A Koopman circuit [27] was connected to the probe with a bias voltage of  $-25$  V and a load resistance of  $3.1 \Omega$ . The signal was observed and recorded on a digital oscilloscope. The pre-pulse at  $t=0$  is due to electron emission from the probe caused by vacuum-ultraviolet emission from the laser induced plasma. The time-of-flight (TOF) from target to probe is determined from the delay between this speed-of-light reference pre-pulse and the maximum voltage rise induced by the arrival of ions in the plume. At the nominal target-substrate distance employed, the time-of-flight of the ions (or molecules) was  $\text{TOF} = 3.4 \pm 0.1 \mu\text{s}$ . The speed of the plume did not slow significantly during propagation, evidenced by a linear best fit to the TOF measured at different distances, Fig. 3a. This highlights that the background gas pressure used had negligible impact on the plume dynamics [28]. As a result, with the further assumption that most of the positive ions have a charge of  $+e$ , we can deduce the energy distribution of the cations for a given deposition distance. The curve in Fig. 3b is computed using the data in Fig. 3a, which reveals a significant fraction ( $\sim 8\%$ ) of ions with energy  $> 100$  eV, sufficient to trigger the island breakup process [18].

From these observations, it is evident that employing energetic PLD coupled with inter-pulse dwell times down to 10 ms, or a continuous deposition frequency of 100 Hz, favoured layer-by-layer growth of  $\text{Sc}_2\text{O}_3$  films. Leading to

high-quality crystal layers that have comparable structural characteristics to those for crystals grown via traditional methods, as will be detailed in the subsequent sections.

### 3.2 Predominance of the $\langle 111 \rangle$ orientation

Example spectra for the XRD measurements of the films deposited at 100 Hz and 2 Hz with an incident  $\text{CO}_2$  laser power of 23 W are presented in Fig. 4a, b. The sample grown at 100 Hz exhibits a strong peak close to  $31.5^\circ$ , i.e., the (222)-peak of  $\text{Sc}_2\text{O}_3$ , and another at  $41.7^\circ$ , the (0006)-peak of  $\alpha\text{-Al}_2\text{O}_3$ , which comes from the sapphire substrate. Aside from the harmonic at  $65.7^\circ$  corresponding to  $\text{Sc}_2\text{O}_3$  (444), there is only one other peak visible in the spectrum (note the log scale used for the y-axis), assigned to  $\text{Sc}_2\text{O}_3$  (332). On the other hand, the XRD pattern for the 2 Hz growth not only presents the same peaks as the 100 Hz growth, but also reveals the appearance of the  $\langle 100 \rangle$ -orientation of  $\text{Sc}_2\text{O}_3$ , as indicated by the (400), (600) and (800) peaks. The calculated ratio between the heights of the (222)-peak and the second strongest orientation is equal to 5320 for the 100 Hz deposition, but only 54 for the 2 Hz deposition. It is also worth mentioning that the second highest peak is not systematically the (400) orientation at other repetition rates but varies from one growth to another.

For the purpose of assessing accurately and objectively the predominance of  $\text{Sc}_2\text{O}_3 \langle 111 \rangle$ -growth, we define a parameter that we will refer to as the ‘area ratio’. To determine this parameter, we take XRD patterns recorded for  $2\theta$  values ranging from  $20^\circ$  to  $80^\circ$ , using the Ge-monochromator and a step-size of  $0.02^\circ$ . We then split the spectra into three zones: the regions corresponding to (1) the  $\text{Sc}_2\text{O}_3$  (222)-peak, (2) the sapphire substrate, and (3) the rest of the spectrum below the  $2\theta$ -angle of  $60^\circ$ .

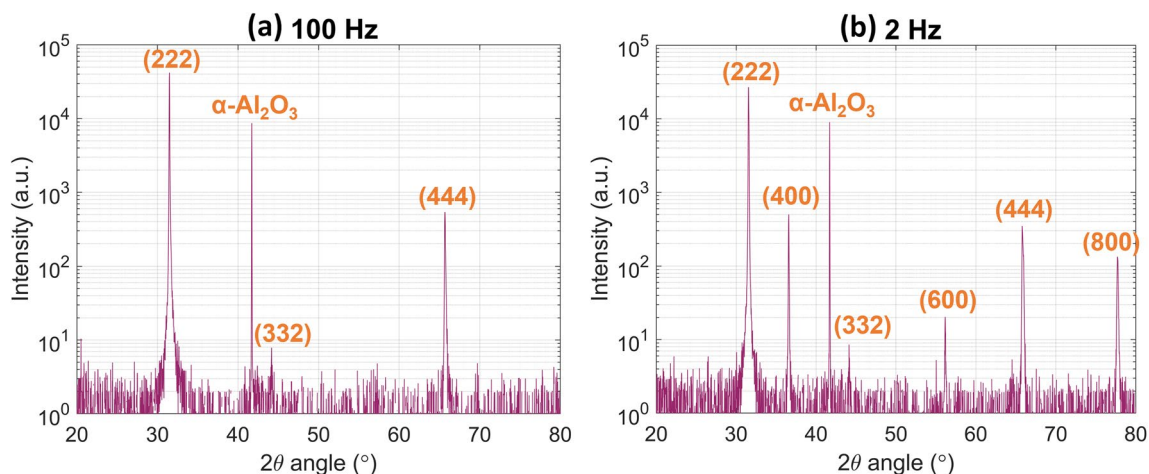


**Fig. 4** XRD patterns for  $\text{Sc}_2\text{O}_3$  thin films grown at: **a** 100 Hz and **b** 2 Hz both at the same  $\text{CO}_2$  laser power of 23 W

The area ratio is defined as the ratio of the area under the spectrum of zones (1) and (3), i.e., the area under the (222)-peak of  $\text{Sc}_2\text{O}_3$  divided by the area of the rest of the diffraction pattern, excluding the substrate peak. As a result, the appearance of additional orientations of  $\text{Sc}_2\text{O}_3$  will directly translate to a decrease in the value of the area ratio. The area under the (222)-peak was calculated for the  $2\theta$  range between  $30^\circ$  and  $33^\circ$  to include the relatively large shoulders of the peak for some of the as-grown films. Zone (2) representing the contribution from the (0006)-peak of the sapphire substrate was delimited between  $41.4^\circ$  and  $42^\circ$ . Note that the (444)-peak of  $\text{Sc}_2\text{O}_3$ , sitting at  $65.7^\circ$ , is outside zone (3) and therefore not included in the calculations. Despite the growth of new orientations at lower repetition rates,  $\text{Sc}_2\text{O}_3$   $\langle 111 \rangle$  remains the most prominent orientation in all the films.

Before calculating the area ratio, a 25-point rolling average was applied to each of the XRD curves minimising the effect of the noise. This distorts the peaks slightly; however, since the noise remains below a signal intensity of four counts, this value was chosen to define the limit between noise and signal. All the points of the smoothed XRD curves with an intensity count above 4 were replaced by the original raw data. This method results in a strong attenuation of the noise with virtually no effect on the shape of the peaks. Finally, the remaining offset of the curves was removed.

For a better understanding of the predominance of the (222)-peak as a function of the repetition rate, a plot of the area ratios for all the samples is displayed in Fig. 5. There is a clear trend showing that, for each substrate heating power,  $\text{Sc}_2\text{O}_3$   $\langle 111 \rangle$ -growth becomes predominant at higher repetition rates. As a relative comparison between the samples, it is noted that the area ratio is higher than 200 for all the depositions above 20 Hz, regardless of the substrate temperature. On the other hand, the film

deposited at 1 Hz with a  $\text{CO}_2$  laser power of 23 W has an area ratio of only 15, revealing the highly textured or polycrystalline nature of this film.

The growth of orientations other than  $\langle 111 \rangle$  appears to be correlated to the 3D growth enabled through longer intervals between pulses. The discontinuities in the crystal surface and the interfaces between different domains, highlighted by the SEM images in Fig. 2, may be the cause for the growth of these other orientations.

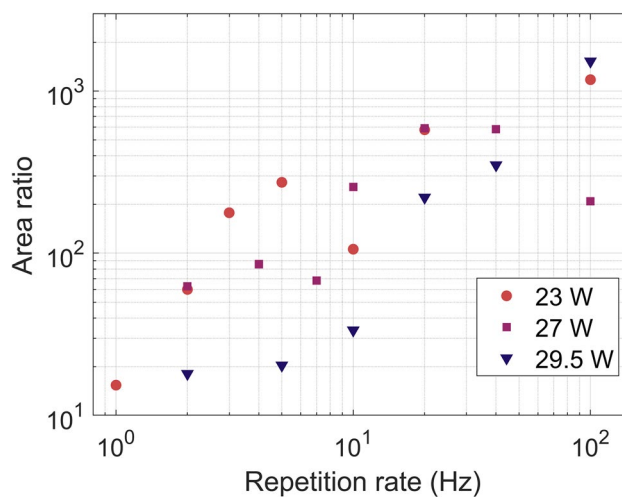


**Fig. 5** Area ratio, defined as the area under the (222) peak divided by the sum of the areas under all the other peaks (see text for the full calculation method). Each point on this graph was calculated from the XRD pattern of a film grown with a specific pulse repetition rate and substrate temperature. Substrate heating powers: 23 W (red circles), 27 W (purple squares), and 29.5 W (blue triangles)



### 3.3 Position of the (222) peak

The relationship between the ablation repetition rate and the lattice constant of the deposited films is directly calculated from the position of the  $\text{Sc}_2\text{O}_3$  (222)-peak in the XRD pattern. However, it was observed that this main peak mostly had an irregular shape with a strong asymmetry, as also seen in [2], therefore determining an exact position of each peak required better definition. Since the position of the peak maximum does not take into consideration its asymmetry, the centre of gravity (CoG) of the peak<sup>1</sup> was selected as the best method to analyse trends in peak position.

A high-resolution XRD scan was performed to analyse the shape and position of the (222)-peak for each sample (step-size of  $0.002^\circ$  and scanning speed of  $1^\circ/\text{min}$ ). The data displayed in Fig. 6a show that the XRD peak moves to higher diffraction angles for reducing repetition rates, which implies a subsequent decreasing in the spacing between lattice planes in a direction normal to the plane of the substrate. From the angle of the CoG maxima, we compute a lattice constant of  $9.838 \text{ \AA}$  for 100 Hz and  $9.809 \text{ \AA}$  for 1 Hz, corresponding to a difference of  $\sim 0.3\%$ . To ensure comparability between the peaks in Fig. 6a, each diffraction pattern was corrected (shifted in  $2\theta$ ) to position the centre of gravity of the substrate's (0006)-peak to  $41.7^\circ$ . This compensates for any unintentional deviation associated with the crystal orientation or sample mounting during the measurement. It is noted that the XRD peak for  $\alpha\text{-Al}_2\text{O}_3$  (0006) has been reported in the literature as between  $41.66^\circ$  and  $41.71^\circ$ . Consequently, our analysis focuses more on the relative position of the  $\text{Sc}_2\text{O}_3$  (222)-peak, rather than its absolute position.

The full-width half maximum (FWHM) of the rocking curves of the films deposited with a heating power of 23 W is plotted in Fig. 6b. The general trend is an increase of the deviation in crystallites orientation for higher repetition rates. One exception was the film deposited at 1 Hz, which may be due to a steady increase in chamber pressure over the 5 h deposition run, noted to have risen to  $\sim 5 \times 10^{-2}$  mbar at the end of the process. Furthermore, a  $5 \times 10^{-2}$  mbar chamber pressure would reduce the kinetic energy of the plume by  $\sim 35\%$  with respect to the standard conditions used, determined by subsequent ion-probe measurements at this background pressure. In-situ post-annealing (for 150 min at deposition conditions) of the film deposited at 100 Hz showed a clear improvement in the rocking curve width. It is also worth noting that the FWHM of the measured rocking curves, of these nominally  $1 \mu\text{m}$ -thick films, are comparable to that of the bulk material, which was reported to be  $0.3^\circ$  [2].

<sup>1</sup> Standard centre of gravity calculation: for a data set of  $N$  points of coordinates  $(x_i, y_i)$ , the centre of gravity is defined by  $\text{CoG} = \frac{1}{N} \sum_i x_i y_i$

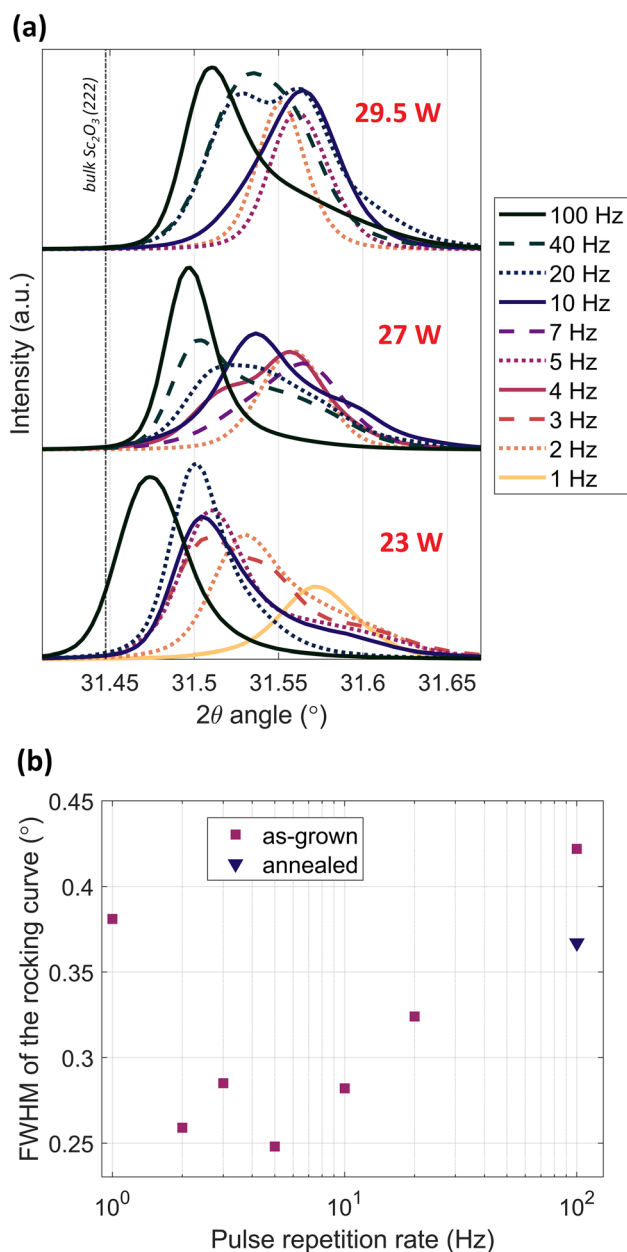


**Fig. 6** a (222) XRD peak of  $\text{Sc}_2\text{O}_3$  films deposited with various repetition rates. The  $\text{CO}_2$  laser powers for substrate heating were: 23 W (bottom), 27 W (middle), and 29.5 W (top). **b** Full width at half maximum of the rocking curves of the samples deposited with 23 W substrate heating. The blue triangle highlights the improvement of the 100 Hz sample after a 150-min post-annealing step at deposition temperature.

Using the centre of gravity definition, Fig. 7 shows the  $\text{Sc}_2\text{O}_3$  (222)-peak position for all the growths performed in this work. Although, for the majority of the as-grown films deposited at low repetition rates ( $\leq 10$  Hz), the CoG remains within the range  $31.545^\circ$ – $31.565^\circ$ , above this frequency, the peak moves to lower angles. It clearly shows that the lattice

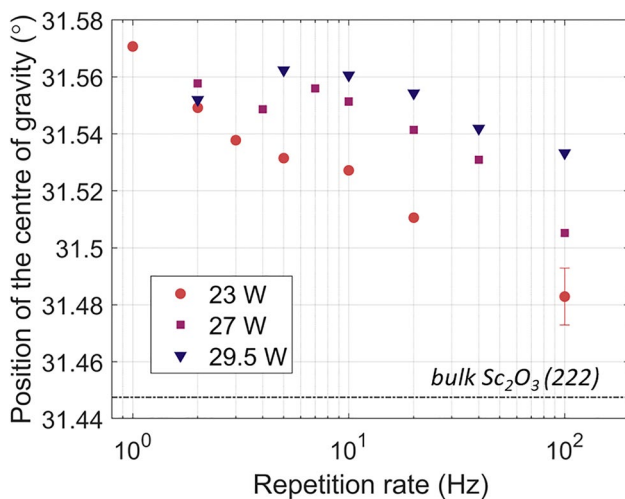


**Fig. 7** Position of the centre of gravity of the (222) peak for all the thin films deposited. The error bar in the lower right corner is valid for all the points in this diagram ( $\pm 0.01$ )

constant approaches that of the bulk material for higher repetition rates.

The error bar in Fig. 7 is indicative for all the data points, based on the angular resolution of the Rigaku SmartLab diffractometer ( $\pm 0.01^\circ$ ). Other sources of uncertainty arise from the fluctuation of the CO<sub>2</sub> laser power and the potential heat-sinking of the substrate holder. Although these are difficult to estimate precisely and cannot be directly translated in terms of uncertainty in the peak position, an error of  $\pm 0.01^\circ$  appears reasonable based on repeatability tests.

An 18,000-shot deposition at 100 Hz only takes 3 min and the power of the CO<sub>2</sub> laser was ramped down immediately at the end of the deposition. On the other hand, a 1 Hz deposition lasts for 5 h, providing quite a substantial time at an elevated temperature and time for the initial layers of the film to anneal and relieve internal stresses. To study the effect of prolonged exposure to high temperatures, two Sc<sub>2</sub>O<sub>3</sub> thin films were deposited on sapphire under identical conditions: a CO<sub>2</sub> laser power of 24 W, an excimer fluence of 1.05 J/cm<sup>2</sup>, and a repetition rate of 100 Hz. One of the samples was in-situ post-annealed for 1 h immediately after deposition with a CO<sub>2</sub> power of 29 W, under a constant  $2 \times 10^{-2}$  mbar O<sub>2</sub> background pressure. The second sample was removed from the chamber after deposition, XRD analysis performed, then several weeks later placed back into the chamber for a 40 min anneal at 29 W (at  $2 \times 10^{-2}$  mbar O<sub>2</sub> background pressure). Note that the heating laser power was ramped up and down over 12 min (each way). The XRD measurements of the (222)-peak for the two samples, plotted in Fig. 8, provide clear evidence that a prolonged exposure at a high temperature has a significant impact on the final (222)-peak position. This observation indicates that the post-annealed film has a smaller lattice constant normal

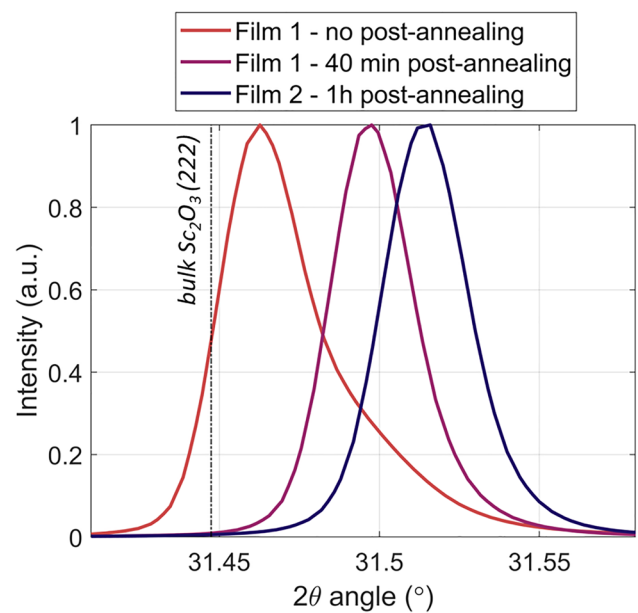


**Fig. 8** XRD spectra for the (222)-peak of Sc<sub>2</sub>O<sub>3</sub> for identical deposition parameters but different post-annealing durations. Red curve: film 1 without annealing. Purple curve: film 1 after 40 min of annealing at 29 W. Blue curve: film 2 with 1 h of annealing at 29 W

to the film plane, which must be compensated by a larger lattice constant parallel to the film plane. Potentially, this is due to the fact that Sc<sub>2</sub>O<sub>3</sub> has a smaller lattice constant than the ideal quasi-lattice-match with the c-plane of sapphire, for which an ideal cubic structure would have a (222)-peak of 30.66°. Consequently, during annealing, the film is stretched in the plane striving to obtain a better match with the sapphire substrate. The shift of the peak position is also accompanied with a decrease in its FWHM, along with an improvement in its symmetry, underlining an improvement in the crystallinity. The reduction of the width of the rocking curve in Fig. 6b also corroborates the idea that annealing relieves defects or strain in the film.

This experiment suggests the explanation as to why the (222)-peak moves to higher angles for lower repetition rates. Above a certain repetition rate threshold, the overall deposition time is too short to give the film enough time to fully relax. Furthermore, this threshold increases with the CO<sub>2</sub>-laser power-substrate temperature (see Fig. 7), which would favour higher diffusion rates and ‘settling’ of the crystal structure more quickly.

The post-annealing effect on the (222)-peak position, along with the appearance of domains (Fig. 2), explains why some of the (222) diffraction peaks in Fig. 6a are composed of multiple sub-peaks. In the XRD measurements, the X-ray beam incident on our samples had a 5 × 5 mm square profile and hence was not sensitive to micron-scale features or structuring. Unlike a single crystal where a



single diffraction peak is realised, a multi-domain highly textured Sc<sub>2</sub>O<sub>3</sub> film will provide a collective response from each of these domains. This will also be constrained by localised domain dimensions and the growth of additional crystal orientations, with their own unique interface conditions. Nevertheless, the FWHM of the peaks range from 0.04° to 0.08°; therefore, in fact, these lattice variations are relatively small, on the order of ~0.15%.

## 4 Conclusion

This report presents a study of PLD growth of crystalline Sc<sub>2</sub>O<sub>3</sub> on <0001>-sapphire substrates. It highlights that the crystalline quality and growth dynamics have a strong dependence upon the deposition pulse repetition rate. The three key film properties of surface topology, level of polycrystallinity, and out-of-plane lattice constant were characterised and related to the deposition conditions, with a prime focus on the pulsed laser repetition rate, or conversely the inter-pulse period. A reduction of the repetition rate favoured the formation of islands and textured crystal growth in the film, as highlighted by SEM images. Ion probe measurements confirmed that more than 8% of the ions in the plume had an energy greater than 100 eV, a level comparable to that required to induce smoothed growth mechanics in energetic PLD of SrTiO<sub>3</sub> [17]. The repetition rate was also shown to be critical in minimising the growth of undesired crystal orientations for the range of substrate temperatures investigated; XRD scans showed that by employing higher repetition rates (20–100 Hz), the growth of <111>-orientated Sc<sub>2</sub>O<sub>3</sub>, the orientation with the smallest lattice mismatch to the substrate, was distinctly favoured. Using an area-ratio analysis of the XRD spectra, a progressive shift was quantified from highly polycrystalline films towards almost purely single-crystal films, with increasing deposition repetition rate. Additionally, the deposited films' out-of-plane lattice constants were determined to increase with increasing repetition rates, observed through the shift in the XRD (222)-peak position. The ostensible reduction of strain (or defect density) in the quasi-lattice-matched hetero-epitaxial system for slow depositions (≤ ~10 Hz) was reproduced with fast depositions (100 Hz) and post-annealing the sample. This protocol consisting of a fast deposition followed by high-temperature annealing benefits from the aforementioned advantages of high-repetition-rate growth, whilst mimicking the strain-relief effects observed in slow depositions. In conclusion, this study demonstrates that faster can indeed be better for high-quality crystal-film growth, which is crucial for realising the deposition rates of interest for real-world applications.

**Acknowledgements** This project has received funding from the European Union's Horizon 2020 research and innovation programme under the Marie Skłodowska-Curie grant agreement No 813159. The authors acknowledge the Engineering and Physical Sciences Research Council (EPSRC) for financial support of the Rigaku SmartLab via grants (EP/K009877/1), (EP/K00509X/1), and (EP/V035975/1), an EPSRC Doctoral Prize EP/T517859/1, and grant nos. EP/N018281/1 and EP/P027644/1. All data supporting this study are openly available from the University of Southampton repository at <https://doi.org/10.5258/SOTON/D1985>.

**Funding** This study was funded by H 2020 (Grant No. 813159), JIM, Engineering and Physical Sciences Research Council (Grant Nos. EP/N018281/1, EP/P027644/1, EP/T517859/1, EP/K009877/1, EP/K00509X/1, EP/V035975/1).

## Declarations

**Ethical approval** The authors confirm that this material is their own original work, which has not been previously published and is not currently being considered for publication elsewhere. The paper reflects the authors' own research and analysis in a clear and honest manner, without any form of data falsification. The authors properly credited all sources and did not appropriate the work of others.

**Open Access** This article is licensed under a Creative Commons Attribution 4.0 International License, which permits use, sharing, adaptation, distribution and reproduction in any medium or format, as long as you give appropriate credit to the original author(s) and the source, provide a link to the Creative Commons licence, and indicate if changes were made. The images or other third party material in this article are included in the article's Creative Commons licence, unless indicated otherwise in a credit line to the material. If material is not included in the article's Creative Commons licence and your intended use is not permitted by statutory regulation or exceeds the permitted use, you will need to obtain permission directly from the copyright holder. To view a copy of this licence, visit <http://creativecommons.org/licenses/by/4.0/>.

## References

1. C. Krankel, Rare-earth-doped sesquioxides for diode-pumped high-power lasers in the 1, 2, and 3 μm spectral range. *IEEE J Sel Top Quant* (2015). <https://doi.org/10.1109/JSTQE.2014.2346618>
2. Y. Kuzminykh, A. Kahn, G. Huber, Nd<sup>3+</sup> doped Sc<sub>2</sub>O<sub>3</sub> waveguiding film produced by pulsed laser deposition. *Opt Mater* **28**(6), 883–887 (2006)
3. T. Gun, Y. Kuzminykh, K. Petermann, H. Scheife, G. Huber, Epitaxial growth by pulsed laser deposition of Er-doped Sc<sub>2</sub>O<sub>3</sub> films on sesquioxides monitored in situ by reflection high energy electron diffraction. *Appl Phys Lett* (2007). <https://doi.org/10.1063/1.2773750>
4. J.J. Prentice, J.A. Grant-Jacob, D.P. Shepherd, R.W. Eason, J.I. Mackenzie, Yb-doped mixed-sesquioxide films grown by pulsed laser deposition. *J Cryst Growth* **491**, 51–56 (2018)
5. A. Suzuki, C. Krankel, M. Tokurakawa, High quality-factor Kerr-lens mode-locked Tm:Sc<sub>2</sub>O<sub>3</sub> single crystal laser with anomalous spectral broadening. *Appl Phys Express* **13**(5), 052007 (2020)
6. F. Rainer, W.H. Lowdermilk, D. Milam, T.T. Hart, T.L. Lichtenstein, C.K. Carniglia, Scandium oxide coatings for high-power UV laser applications. *Appl Opt* **21**(20), 3685–3688 (1982)

7. S. Tamura, S. Kimura, Y. Sato, H. Yoshida, K. Yoshida, Laser-damage threshold of  $\text{Sc}_2\text{O}_3/\text{SiO}_2$  high reflector coatings for a laser wavelength of 355 nm. *Thin Solid Films* **228**(1–2), 222–224 (1993)
8. J. Du, J. Wang, G.A. Hart, J.F. Oudard, Investigation of  $\text{Sc}_2\text{O}_3$  for high laser durability ultraviolet coating applications. *Proc SPIE* **89**(9), 10691 (2018)
9. A.M. Herrero, B.P. Gila, C.R. Abernathy, S.J. Pearton, V. Craciun, K. Siebein, F. Ren, Epitaxial growth of  $\text{Sc}_2\text{O}_3$  films on GaN. *Appl Phys Lett* **89**(9), 092117 (2006)
10. J.W. Johnson, B.P. Gila et al.,  $\text{SiO}_2/\text{Gd}_2\text{O}_3/\text{GaN}$  metal oxide semiconductor field effect transistors. *J Electrochem Soc* **148**(6), G303–G306 (2001)
11. C. Liu, E.F. Chor, L.S. Tan, A. Du, Epitaxial growth of  $\text{Sc}_2\text{O}_3$  films on GaN (0001) by pulsed laser deposition. *J Vac Sci Technol B* **25**(3), 754–759 (2007)
12. L. Tarnawska, A. Giussani et al., Single crystalline  $\text{Sc}_2\text{O}_3/\text{Y}_2\text{O}_3$  heterostructures as novel engineered buffer approach for gan integration on Si (111). *J Appl Phys* **108**(6), 063502 (2010)
13. M. Stehlik, G.A. Govindassamy, J. Zideluns, F. Lemarchand, F. Wagner, J. Lumeau, J.I. Mackenzie, L. Gallais, Sub-picosecond 1030 nm laser-induced damage threshold evaluation of pulsed-laser deposited sesquioxide thin-films. *Opt Eng* (2022). <https://doi.org/10.1117/1.OE.61.7.070903>
14. J. Paulraj, R.P. Wang, M. Sellars, B. Luther-Davies, Epitaxial growth of  $\text{Sc}_2\text{O}_3$  films on  $\text{Gd}_2\text{O}_3$ -buffered Si substrates by pulsed laser deposition. *Appl Phys A Mater* (2016). <https://doi.org/10.1007/s00339-016-9968-z>
15. C. Liu, E.F. Chor, L.S. Tan, Y.F. Dong, Structural and electrical characterizations of the pulsed-laser-deposition-grown  $\text{Sc}_2\text{O}_3/\text{GaN}$  heterostructure. *Appl Phys Lett* **88**(22), 222113 (2006)
16. S.Q. Zhang, R.F. Xiao, Yttrium oxide films prepared by pulsed laser deposition. *J Appl Phys* **83**(7), 3842–3848 (1998)
17. P.R. Willmott, R. Herger, C.M. Schlepütz, D. Martocchia, B.D. Patterson, Energetic surface smoothing of complex metal-oxide thin films. *Phys Rev Lett* **96**(17), 176102 (2006)
18. J.G. Ulbrandt, X. Zhang, R.L. Headrick, R. Liu, M. Dawber, K. Evans-Lutterodt, Fast nonthermal processes in pulsed laser deposition. *Phys Rev B* **101**(24), 241406 (2020)
19. G. Eres, J.Z. Tischler, C.M. Rouleau, H.N. Lee, H.M. Christen, P. Zschack, B.C. Larson, Dynamic scaling and island growth kinetics in pulsed laser deposition of  $\text{SrTiO}_3$ . *Phys Rev Lett* **117**, 206102 (2016)
20. D.H.A. Blank, G. Koster, G.A.J.H.M. Rijnders, S. Eelco van, P. Slycke, H. Rogalla, Epitaxial growth of oxides with pulsed laser interval deposition. *J Cryst Growth* **211**(1), 98–105 (2000)
21. G. Eres, J.Z. Tischler, C.M. Rouleau, P. Zschack, H.M. Christen, B.C. Larson, Quantitative determination of energy enhanced interlayer transport in pulsed laser deposition of  $\text{SrTiO}_3$ . *Phys Rev* (2011). <https://doi.org/10.1103/PhysRevB.84.195467>
22. S. Bar, G. Huber, J. Gonzalo, A. Perea, A. Climent, F. Paszti, Europium-doped sesquioxide thin films grown on sapphire by PLD. *Mat Sci Eng B Solid* **105**(1–3), 30–33 (2003)
23. A. Jain, S.P. Ong et al., Commentary: the materials project: a materials genome approach to accelerating materials innovation. *APL Mater* **1**(1), 011002 (2013)
24. J.J. Prentice, J.A. Grant-Jacob, S.V. Kurilchik, J.I. Mackenzie, R.W. Eason, Particulate reduction in PLD-grown crystalline films via bi-directional target irradiation. *Appl Phys A Mater* (2019). <https://doi.org/10.1007/s00339-019-2456-5>
25. T.C. May-Smith, A.C. Muir, M.S.B. Darby, R.W. Eason, Design and performance of a ZnSe tetra-prism for homogeneous substrate heating using a  $\text{CO}_2$  laser for pulsed laser deposition experiments. *Appl Opt* **47**(11), 1767–1780 (2008)
26. A. Sposito, *Pulsed laser deposition of thin film magneto-optic materials and lasing waveguides* (University of Southampton, Physical Sciences and Engineering, 2014)
27. D.W. Koopman, Langmuir probe and microwave measurements of properties of streaming plasmas generated by focused laser pulses. *Phys Fluids* **14**(8), 1707–2000 (1971)
28. A. Sambri, S. Amoruso, X. Wang, F.M. Granozio, R. Bruzzese, Plume propagation dynamics of complex oxides in oxygen. *J Appl Phys* **104**(5), 053304 (2008)

**Publisher's Note** Springer Nature remains neutral with regard to jurisdictional claims in published maps and institutional affiliations.